JOURNAL OF MATERIALS SCIENCE 18 (1983) 998–1004

Microchemistry and microstructure of a multiphase aluminosilicate ceramic

SUBHASH H. RISBUD
Department of Ceramic Engineering and Materials Research Laboratory, University of Illinois at Urbana-Champaign, Urbana, IL 61801, USA

AVIGDOR ZANGVIL
Materials Research Laboratory and Department of Metallurgy and Mining Engineering, University of Illinois at Urbana-Champaign, Urbana, IL 61801, USA

The microstructure and microchemistry of a sintered ($\approx$ 1700° C) aluminosilicate ceramic (60 wt % Al_2O_3–40 wt % SiO_2) was investigated by optical, scanning (SEM and EDAX), and analytical electron microscopy (TEM and STEM). The microstructural features of the fired ceramic consisted of unreacted Al_2O_3, glass, porosity, and equilibrium and metastable mullite phases. Residual Al_2O_3 agglomerates ($\approx$ 15 to 30 μm in size) were surrounded by a $\approx$ 6 μm layer of equilibrium mullite ($\approx$ 71.3 to 73.5 wt % Al_2O_3). The unreacted Al_2O_3–equilibrium mullite assembly formed islands embedded in a silica rich glass ($\approx$ 4.5 to 14 wt % Al_2O_3) which also contained 2 to 3 μm thick metastable mullite needles ($\approx$ 70 to 77 wt % Al_2O_3). Phase separation and alumina rich glass compositions ($\approx$ 57 to 59 wt % Al_2O_3) were also observed in some areas of the microstructure.

1. Introduction

Ceramic materials are characteristically multiphasic in nature. The result of usual ceramic processing techniques, involving pressing and firing, leads to a microstructure containing crystals, solid solution phases, glasses and often, unavoidably, some degree of porosity. The properties of ceramics are thus affected by the nature and distribution of this multiphase assemblage and is possibly influenced by phase location as well. Thus, microstructural analysis of ceramic phases and the association with relevant stable or metastable phase equilibria data is a very significant aspect of ceramic materials development activity.

In the present study we report results of the microstructure and microchemistry of an aluminosilicate ceramic (60 wt % Al_2O_3–40 wt % SiO_2) in which reactions to the final stable equilibrium configuration have not reached completion. The composition chosen is close to commercial fireclay and high alumina mullite refractories and to naturally occurring sillimanite ($Al_2O_3 \cdot SiO_2$). Studies of diffusion and reactions under controlled processing conditions have resulted in several useful determinations of stable and metastable phase equilibria in the SiO_2–Al_2O_3 system [1–6]. The motivation of the present investigation, however, is to better characterize the microchemistry and microstructure of phases developed under firing conditions customarily used for refractory bodies. Thus, no deliberate attempt to attain phase equilibrium was made and microstructural analysis was the focus of the work. Optical microscopy, electron microprobe, and scanning, transmission and scanning transmission electron microscopy (SEM, TEM, STEM, respectively) were the principal characterization techniques employed.

2. Experimental procedures

2.1. Materials preparation

Powders of reactive A-16* alumina and high purity fused silica,† (corresponding to a composition of 60 wt % Al_2O_3–40 wt % SiO_2) were thoroughly mixed by dry milling in a plastic bottle with

*ALCOA, Aluminum Co. of America, Pittsburgh, PA.
†325 mesh Corning #7940, Corning Glass Works, NY.

0022–2461/83 $03.00 + .12

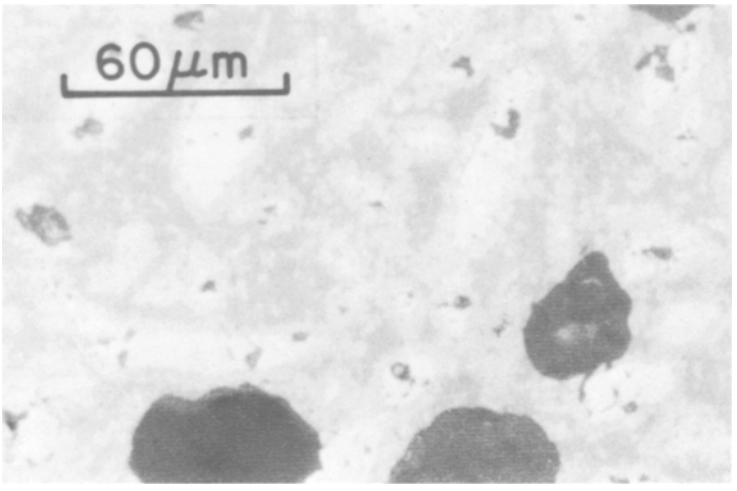

Figure 1 Optical micrograph of sintered aluminosilicate ceramic (60 wt % Al_2O_3–40 wt % SiO_2) showing unreacted alumina (white areas), mullite layers (next to the alumina), mullite needles embedded in a siliceous glass matrix (dark grey regions) and porosity (black areas).

alumina grinding media for about 24 h. The mixture was dry pressed into pellets and fired in a platinum crucible in air at about 1700° C for 96 h. The fired pellets had dimensions of about 2 cm diameter x 0.75 cm thickness.

2.2. Optical and scanning electron microscopy

Samples from the as-fired pellet were cut on a diamond saw and prepared for optical microscopy. Ceramographic polishing procedures consisted of approximately 10 to 15 min of grinding on each 30, 15 and 6 μm metal-bonded diamond wheel, 48 to 50 h of vibratory polishing‡ using 6 and 1 μm diamond particles, and a final polish for about 48 h using a 1/4 μm slurry of diamond particles. The highly polished samples were observed in reflected light by interference-contrast micrography.§ A light etch of 10% HF was necessary to observe the microstructure. Specimens for scanning electron microscopy consisted of the fracture surfaces of samples on which a thin film of gold was evaporated prior to examination.

2.3. TEM and microanalysis

Samples for transmission electron microscopy were prepared by slicing off about 250 μm thick slices, mechanically polishing down to 70 to 100 μm on rotating SiC paper discs (grit 180, 240, 320) then producing a 3 mm disc with the aid of a sand abrasive machine, and finally argon ion thinning to perforation. All samples were coated with a thin layer of gold or carbon to suppress charging. The samples were studied on a JEOL JSEM 200 scanning transmission electron microscope (STEM) equipped with an ORTEC energy-dispersive X-ray spectrometer (EDS) for elemental analysis. This instrument was fitted by Zaluzec and Fraser [7] with a graphite specimen cup and a brass liner above the objective lens to greatly reduce X-ray fluorescence effects and reduce the peaks due to the systems to low values.

3. Results

3.1. Ceramography, microprobe and SEM

The overall microstructure of the as-fired ceramic is shown in Fig. 1. The white areas in the optical micrograph show sintered Al_2O_3 particles which are surrounded by a light grey layer of mullite that must have formed at 1700° C by a diffusion controlled reaction with the siliceous liquid. The thickness of the mullite layer adjacent to the sintered Al_2O_3 particles is about 6 μm after 96 h of reaction. The diffusion controlled nature of the reaction through the mullite layer is indicated in the slow rate observed. The composition of the mullite layer was determined by the electron beam microprobe to be about 70.6 wt % Al_2O_3 which corresponds to the stable equilibrium composition [2]. The liquid phase next to the mullite layer has a composition of about 11 wt % Al_2O_3.

Precipitation of mullite needles in the liquid phase was also observed as shown in Fig. 2. These needles formed during the quench from 1700° C after holding at the temperature for 96 h. The microstructure shown in Figs. 1 and 2 is interesting

‡Syntron Div., FMC Corp., Homer, PA.
§Nomarski interference-contrast microscope, Zeiss Ultraphot II, Carl Zeiss, West Germany.

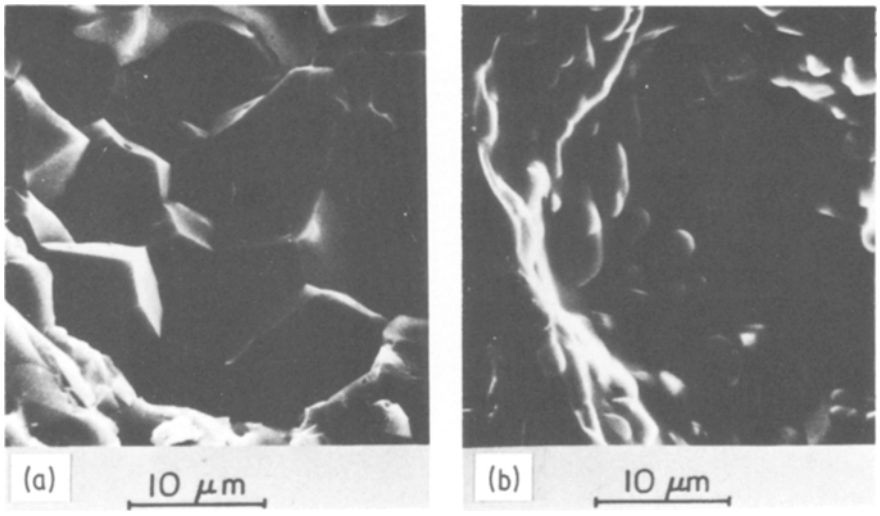

Figure 2 SEM micrographs showing a closer view of unreacted alumina regions (a) and mullite needles in glass matrix (b).

in that two different mullite morphologies can be seen in the same sample. The scanning electron micrographs of Fig. 2a show the sintered Al_2O_3 particles with fragments of the mullite layer. The mullite growing out of the liquid phase as isolated needle-like islands is shown in Fig. 2b. The relative ratio of Al/Si in the two mullites was determined by the EDAX (Energy Dispersive Analysis of X-rays) attachment to the scanning electron microscope. The Al/Si intensity ratios are shown in Fig. 3 by focusing the beam (about 1 μm diameter) on the sintered Al_2O_3 area (Fig. 2a) and on the mullite needles in the liquid phase matrix (Fig. 2b). The higher Al/Si ratio in Fig. 2b is semi-quantitative evidence of a higher Al_2O_3 mullite precipitating from a liquid phase. A rough estimate of the Al/Si ratio in the two mullites can be made simply from the peak heights and gives a value of Al/Si about 2 for the equilibrium mullite layer and Al/Si about 3 for the mullite needles in the glass matrix.

3.2. Transmission electron microscopy

Due to the different milling rates of the phases in the material, it was virtually impossible to obtain an electron-transparent thin area which contained all the phases of interest. Usually, each thin area had only two of these phases. It was, therefore, necessary to study of large number of such areas in order to fully interpret the microstructural and microchemical features. The identity of each phase was determined by semi-quantitative analysis of aluminum and silicon and confirmed by selected area electron diffraction (SAD) or microdiffraction techniques. In addition, more accurate quantitative analysis was accomplished for all the observed phases.

Fig. 4 shows a TEM of the equilibrium mullite layer which surrounds an alumina agglomerate. The interesting feature is the porous interface area, which may be a result of the higher density of the reaction product (mullite) as compared to

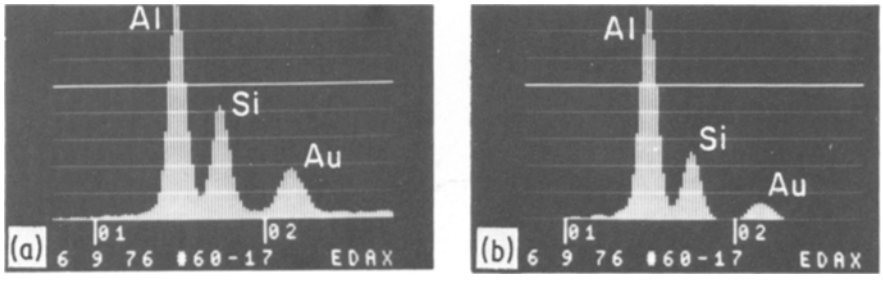

Figure 3 EDAX spectra from mullite layer next to unreacted alumina regions (a) and from mullite needles (b). The differences in the Al/Si ratios in the two mullites are evident.

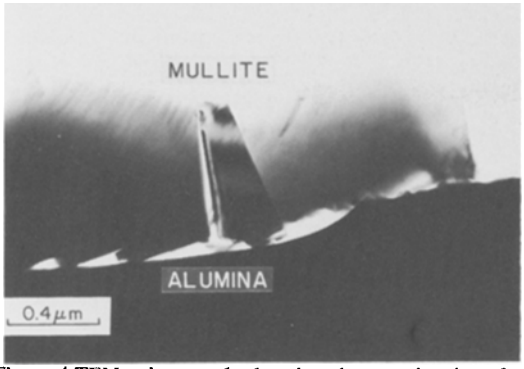

Figure 4 TEM micrograph showing the reaction interface between mullite layer and alumina.

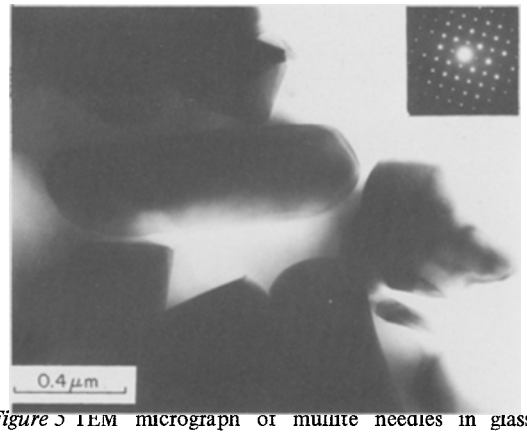

Figure 5 TEM micrograph of mullite needles in glass matrix and selected area diffraction pattern (inset) from the needles.

the original weighted average density of the Al_2O_3 and the liquid, assuming that some siliceous liquid is trapped near the interface during the reaction process. Fig. 5 shows a typical area of metastable mullite needles embedded in a SiO_2-rich glass, with an SAD pattern of one of the needles. Such areas constituted a good part of the microstructure and occurred quite frequently. The needles have nearly-square cross-sections, sometimes rounded, with their long axis paralled to the [0 0 1] direction of the orthorhombic structure. All the mullite needles, as well as the equilibrium mullite grains, could be indexed according to the reported orthorhombic structure with a nearly tetragonal unit cell measuring $a = 0.755$ nm, $b = 0.769$ nm and $c = 0.2884$ nm. Extinctions for $(h\,0\,0)$ and $(0\,k\,0)$ could be observed for odd values of h or k, in agreement with the reported space group (Pbam).

An additional feature of the microstructure is the appearance of Al_2O_3-rich glass areas, measuring from a few micrometres to over 10 μm. By analysing compositions and SAD patterns along edges of holes in the TEM sample and measuring the extent of each phase at low magnifications it could be established that the Al_2O_3-rich glass was always in contact with mullite and that the two most prevalent sequences were Al_2O_3-rich glass/mullite/SiO_2-rich glass and Al_2O_3/mullite/Al_2O_3-rich glass. Phase separation was also infrequently observed in some of the Al_2O_3-rich glass areas, as shown in Fig. 6.

3.3. STEM microanalysis

The composition of the various phases was deter-

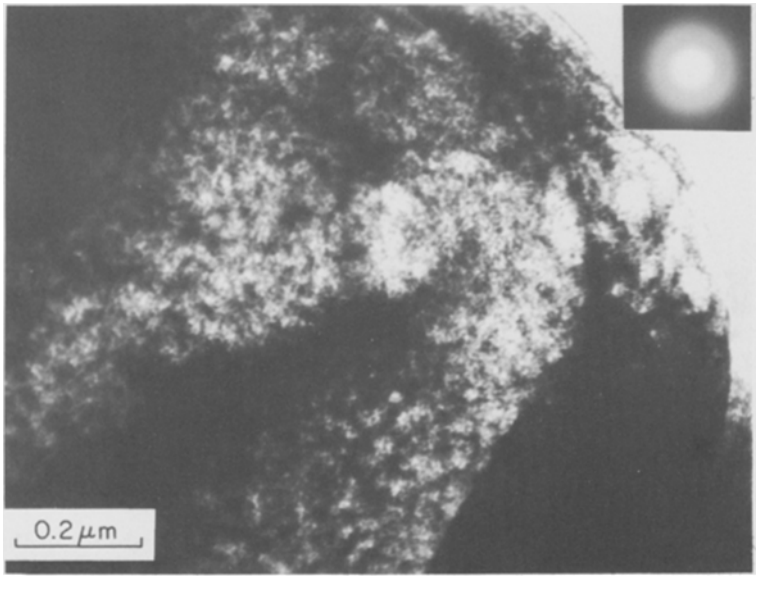

Figure 6 Example of glass-in-glass phase separated area in the microstructure. SAD pattern confirms the amorphous nature of this region.

TABLE IA Summary of microchemical analysis. Electron microprobe

Equilibrium mullite layer composition	≈ 70.6 wt % or 58.5 mol % Al_2O_3
Glass matrix (with mullite needles) composition	≈ 11.0 wt % Al_2O_3 or 6.7 mol % Al_2O_3

mined by a standardless quantitative analysis of aluminum and silicon in the thin foil, combined with the assumption that stoichiometric SiO_2 and Al_2O_3 are the only possible components. Each EDS spectrum was corrected by subtraction of the in-hole spectrum (usually negligible) and the computer-fitted background. The $K\alpha$ peaks were then approximated to Gaussian by a least square method and the ratio of the integrated intensities (between points of half peak height) was used as the $K\alpha$ ratio, subsequently corrected according to the atomic number and detector efficiency. An absorption correction was also performed, but it was found unnecessary for foil thicknesses below about 250 nm. The STEM results and previously discussed electron microprobe analyses are summarized in Tables IA and IB. The values for the equilibrium mullite, 71.3 to 73.5 wt% Al_2O_3, were highly reproducible and in excellent agreement with the reported 70 to 73% range of stable mullite [2]. The metastable mullite needles had a much wider range of composition and could be divided into a high-Al_2O_3 and a low-Al_2O_3 group. The SiO_2-rich glass matrix varied in composition from one region to the other, between 4.5 and 14 wt% Al_2O_3 while the Al_2O_3-rich glass composition was far less variable. Areas with phase separation adequate for analysis were small in number and reliable quantitative results could not be obtained. They were, however, generally close in composition to the Al_2O_3-rich glass.

4. Discussion

Two significant reactions could be considered responsible for the microstructural features observed in this work. During the firing of the pressed ceramic at 1700° C for about 96 h the partially sintered alumina particles start to react with a siliceous liquid to form mullite by a solid state reaction as suggested by the SiO_2–Al_2O_3 stable phase equilibrium diagram [2] shown in Fig. 7. The average compositon of this mullite layer (see Fig. 1) as determined by electron microprobe is 70.6 wt% Al_2O_3 and is thus consistent with the stable mullite solid solution composition. STEM measurements also confirm this result and can thus be treated as an internally consistent calibration point for the STEM analysis.

Continued growth of the mullite layer is dependent on the continuation of the reaction between alumina and the siliceous liquid. Since diffusion data indicate considerable sluggishness in these systems, the sintered alumina island (about 20 to 30 μm) is left unreacted even after 96 h of contact with this silicate liquid, although the stable equilibrium phases predicted by the phase diagram should be mullite plus liquid.

During the cooling of the pellet after the 96 h firing cycle the metastable mullite–alumina–liquid assembly solidifies with the rapid crystallization of relatively high-alumina needles of mullite solid solution. Some needles exhibit as much as 77 wt% Al_2O_3 while others seem to be much lower in alumina (about 70 to 73 wt%). The latter result might be explained in terms of the inhomogeneity of local composition in the siliceous liquid prior to quenching. The morphological and chemical nature of the mullite needles is consistent with the proposed SiO_2–metastable mullite pseudobinary system suggested by Aksay and Pask [2].

TABLE IB Summary of microchemical analysis. STEM analysis (corrected for absorption, etc.)

Microstructure phase	Chemical composition		Number of analyses
	mol % Al_2O_3	wt % Al_2O_3	
1. Unreacted alumina	> 98.5	> 99.0	> 10
2. Mullite layer	59.4 to 62.0	71.3 to 73.5	10
3. Mullite needles	63.8, 66.1	75, 76.8	2
(2 groups)	57.9 to 60.7	70 to 73	9
4. Glassy phases:			
(a) Silica-rich glass	3 to 8.9	4.5 to 14	6
(b) Alumina-rich glass	44 to 46	57 to 59	4

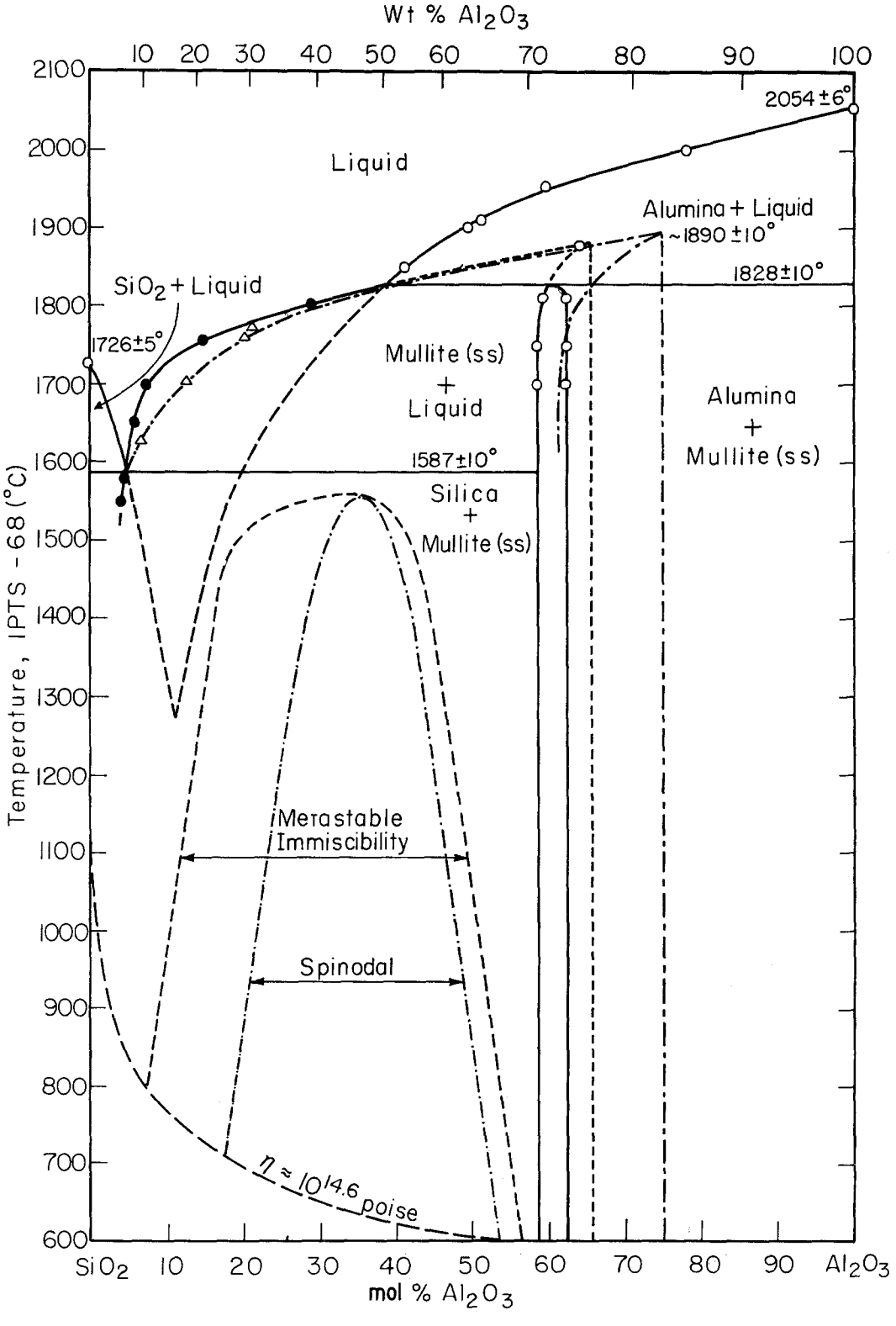

Figure 7 $SiO_2-Al_2O_3$ phase diagram showing stable and metastable equilibrium curves (after [2] and [6]) and a proposed liquid miscibility gap (after [5]).

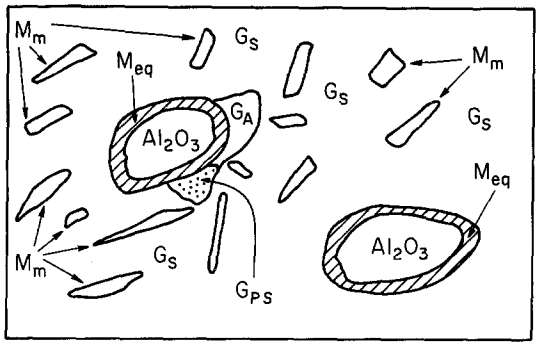

Figure 8 Schematic sketch of phase distributions in the sintered ceramic as deduced from present microstructural study. M_{eq} = equilibrium mullite; M_m = metastable mullite needles; G_s = silica-rich glass; G_{ps} = phase separated glass; G_A = alumina-rich glass.

Secondary in importance, in terms of their abundance in the microstructure, are the Al_2O_3-rich glassy areas. An approximate calculation shows that their composition should be similar to the average composition of the glass/metastable-mullite regions. We suggest that the high-temperature siliceous glass, prior to cooling, is considerably inhomogeneous in composition. Local composition should be affected by such factors as the vicinity of retained Al_2O_3 islands or of equilibrium mullite, because glassy areas near the equilibrium mullite would tend to be relatively richer in Al_2O_3. In addition, inhomogeneities must also develop upon cooling, according to differences in local nucleation and growth rates of metastable mullite, which are, in turn, enhanced by differences in local cooling rates. All these factors appear to contribute to the complicated microstructure. Thus, areas with similar compositions (about 50% Al_2O_3) may result in either glass + mullite or Al_2O_3-rich glass or phase separated glass, according to local circumstances. One might suggest, based on the metastable phase diagram (Fig. 7) that locally high compositions result in glass + mullite needles, while lower compositions remain as Al_2O_3-rich glass or undergo phase separation upon cooling. However our micro-analysis indicates that the Al_2O_3-rich glass is very close in composition (57 to 59 wt % Al_2O_3) to the calculated average composition of glass + mullite areas (56 to 58 wt % Al_2O_3 based on estimated 5 to 10% residual alumina and the known overall composition), which suggests that local cooling rates and nucleation sites may be more important factors than the local composition itself. It is worthwhile re-emphasizing that such non-equilibrium microstructures, rather than equilibrium structures, are more likely to develop in many commercial heat treatments of refractory ceramics.

Fig. 8 is a schematic view of the phases present in the microstructure and their possible relative arrangement. This picture can explain our observed sequence of phases. There is no doubt about the arrangement of residual Al_2O_3, SiO_2-rich matrix and metastable mullite needles, as these were observed independently by optical microscopy and SEM. The locations of Al_2O_3-rich glass and phase separated glass were derived indirectly from TEM observation and could not be otherwise confirmed. Al_2O_3-rich glass areas were observed to appear in contact with large mullite areas (equilibrium mullite) on one side and SiO_2-rich glass or Al_2O_3 on the other side, as depicted in the sense of a statistical result in Fig. 8. It is possible that some Al_2O_3-rich glass or phase separated glass areas occur in other locations in the microstructure as well.

Acknowledgements

This research was supported by the Materials Sciences Division of the US Department of Energy under contract DE-AC02-76ER01198 and was conducted in the facilities of the Center for Microanalysis of Materials in the Materials Research Laboratory at Urbana.

References

1. R. F. DAVIS and J. A. PASK, *J. Amer. Ceram. Soc.* 55 (1972) 525.
2. I. A. AKSAY and J. A. PASK, *ibid.* 58 (1975) 507.
3. S. ARAMAKI and R. ROY, *ibid.* 42 (1959) 644.
4. *Idem, ibid.* 45 (1962) 229.
5. S. H. RISBUD and J. A. PASK, *ibid.* 60 (1977) 418.
6. *Idem, J. Mater. Sci.* 13 (1978) 2449.
7. N. J. ZALUZEC and H. L. FRASER, *J. Phys. E.* 9 (1976) 1051.

Received 18 March
and accepted 29 July 1982